Lasers in Manufacturing Conference 2019

Direct Laser Interference Patterning of antibacterial surfaces on stainless steel by means of ultrafast laser

Alexander Peter[a,*], Adrian H.A. Lutey[b], Sebastian Faas[a], Luca Romoli[b], Volkher Onuseit[a], Thomas Graf[a]

[a]*Institut für Strahlwerkzeuge (IFSW), University of Stuttgart, Pfaffenwaldring 43, 70569 Stuttgart, Germany*
[b]*Dipartimento di Architettura e Ingegneria, University of Parma, Parco Area delle Scienze 181/A, 43124 Parma, Italy*

Abstract

Direct Laser Interference Patterning (DLIP) is a laser processing method that provides a tool for creating a wide field of functional surfaces. In the present work, the generation of antibacterial surfaces on stainless steel is shown with a high power capable DLIP setup. The used laser was an ultrafast laser with a wavelength of 1030nm and a pulse duration of eight picoseconds. Two different topographies were produced, which were generated with two different polarization orientation of the laser. Both topographies were investigated in their antibacterial behavior. The employed method for assessing the bacterial retention is based on ISO standards for measurement of antibacterial performance. The resulting topographies shows a retention of up to 99,8% for E. Coli and up to 79.1% for S. aureus bacteria.

Keywords: direct laser interference patterning; two beam interference; functional surfaces; antibacterial surfaces; ultrafast laser; stainless steel;

1. Introduction

Functional surfaces are of growing interest such as in food and healthcare industries [1,2]. In such critical applications, sophisticated cleaning routines are necessary to ensure bacterial contamination requirements

* Corresponding author. Tel.: +49-711-685-69743.
E-mail address: alexander.peter@ifsw.uni-stuttgart.de.

are met [3]. Functional surfaces are therefore interesting to not only reduce the contamination, but also for simplify cleaning procedures.

Several methods, such as plasma etching, anodic oxidation, chemical vapor deposition, lithography and electrospinning facilitate the production of surfaces with antibacterial behavior [4]. Laser-based methods to produce functional surfaces have also been demonstrated in recent works [5, 6, 7, 8], which facilitate the production of large areas in a single step process by means of ultrashort lasers [9,10,11]. Linearly polarized laser pulses and surface plasmons effect Laser Induced Periodic Surface Structures (LIPSS) perpendicular to the orientation of the polarization with a ridge separation in the order of the wavelength [12, 13]

Beside LIPSS, Direct Laser Interference Patterning (DLIP) is another promising laser based method to produce functional surfaces. In contrast to LIPSS, DLIP exploits ablation of periodic topographies by means of an interference pattern, dependent on the number of interfering beams, incidence angle, fluence and polarization orientation [14, 15, 16, 17]. Furthermore, the combination of DLIP and LIPSS leads to topographies that may differ from the interference pattern itself [18, 19].

In the present work, the DLIP method was employed to generate two different antibacterial topographies on 50x50mm^2 large stainless steel samples by means of two-beam interference with combination of the LIPSS effect. Due to current developments of high power laser sources at a wavelength of 1030 nm [20,21,22], a 1030 nm high power capable DLIP optical setup, designed in a previous work [23], was employed. This capability promises high structuring rates in the future.

The resulting topographies were analyzed by means of a scanning electron microscope (SEM). Finally, the topographies were tested for antibacterial behavior with Escherichia coli (E. coli) and Staphylococcus aureus (S. aureus) bacterial cells.

2. Material and methods

2.1. Optical setup

For the structuring process a DLIP Setup, shown in [23], was employed. This setup provides DLIP with up to 4 beams and variation of interference pattern period, spot diameter on the sample surface and polarization of each beam independently. Furthermore, the optical setup was designed for high pulse energies.

Fig. *1* shows a schematic of the setup in case of two beams interference patterning. The laser beam is fed from above through a variable telescope and is then split by a diffractive beam splitter into two beams with a total angle of 18.6°. Two inner mirrors guide the two beams through λ/half plates, to allow the variation of the polarization of each beam. The following two mirrors reflect the two beams into one spot on the sample surface, where the interference patterns occur. The outer mirrors are mounted on mechanical goniometers to provide the variation of the incidence angle and therefore the interference period on the sample surface. The sample is fixed on axes, which move the sample for large area structuring.

The intensity distribution of two coherent interfering beams is described in x-direction as [14]

$$I(x,y) = 2I_0\left[1+\cos\left(\frac{4\pi\sin(\theta)}{\lambda}x\right)\right], \quad (1)$$

with the intensity of each beam I_0, the wavelength λ of the interfering beams and their incidence angle related to the surface normal θ as shown in Fig. *1*. This formula applies with the following assumptions: same angle of incidence related to the surface normal in x-direction, same intensity and same polarization angle for each beam.

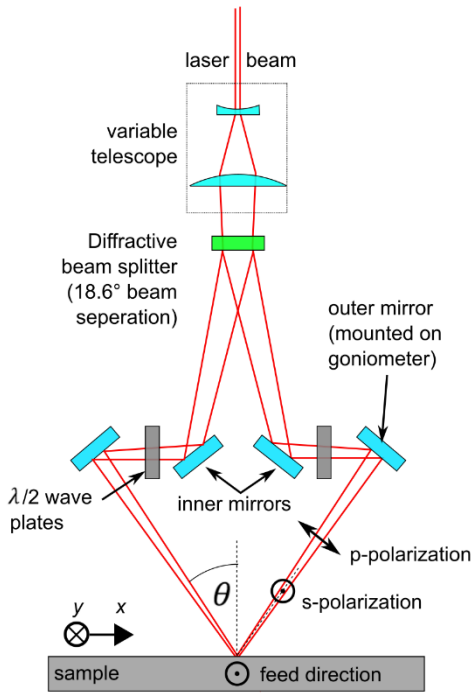

Fig. 1: Schematic of the used Direct Laser Interference Patterning setup.

From the argument of the cosine it is evident that the period of the interference pattern Λ depends on the angle with [14]

$$\Lambda = \frac{\lambda}{2\sin(\theta)}. \tag{2}$$

Based on investigations from [24] the structure period has to be in the range of the size of E. Coli and S. aureus. Therefore, a period of about 850nm was chosen. On the one hand, the half period is smaller than the cells and on the other hand, the limits of the optical setup, regarding the incident angle, are not exhausted. This period and the wavelength of 1030nm requires applied to eq.(*2*) an incidence angle of 37°.

In Fig. *2* a comparison between the calculated and measured interference pattern, resulting from 37° incidence angle, is shown. The calculation is based on eq.(*1*), pictured on the left hand side. On the right hand side, the measurement at the beams overlapping area on the sample surface after the DLIP setup is pictured. Applicable for both, the x- and y-axis represent the positon of the sample surface, where the two beams interfere. Intensity distribution of the pattern is colored corresponding to the color bar to the right of the plot. For the measurement, the interference pattern was magnified with a 50x microscope objective and acquired with a 5µm pixel size camera chip. In comparison, it is obvious that the measurement has a clear correlation with the calculated interference pattern.

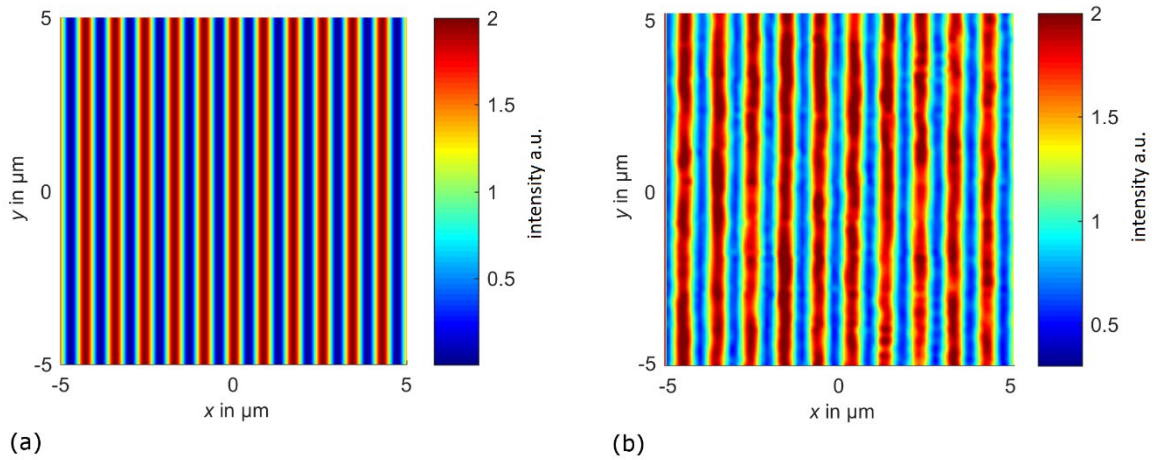

Fig. 2: Comparison of calculated and measured interference patterns. On the left hand side, the eq(1) based intensity distribution is shown. On the right hand side the measured Intensity distribution. The measurement was employed by means of an 50x microscope objective and an IDS uEye UI-2220-M camera.

2.2. Process strategy

For structuring large areas, a strategy with continuous feed rate, parallel to the interference lines was chosen and a suitable pulse overlap to reach the required depth of the structure topography with a sufficient number of pulses at one location. The average fluence of the entire beam cross section at the sample surface were set to 0.1 J/cm^2.

In this case, the required number of pulses and the large area structuring strategy with a continuous moving sample, the feed rate and the repetition rate were determined. As a consequence of the spot size d_s of 60µm in the feed direction, the repetition rate f_{rep} of 100kHz and the required 60 pulses N_p at one location the feed rate v_f needed to be set to

$$v_f = \frac{f_{rep} \cdot d_s}{N_p} = 100 \, \frac{\mathrm{mm}}{\mathrm{s}}. \tag{3}$$

To nevertheless get 2D structures with 1D interference pattern, a second process step was performed. This step consists of the same structuring process as the first, except with an additional perpendicular structuring direction on the sample with half the pulse energy. Between the two steps, the sample was rotated 90° (schematically shown in Fig. 3). In consideration of the dependents of material absorption on its roughness, the pulse energy of the second step was reduced to half. With this setting a balanced topography in the x and y directions could be reached.

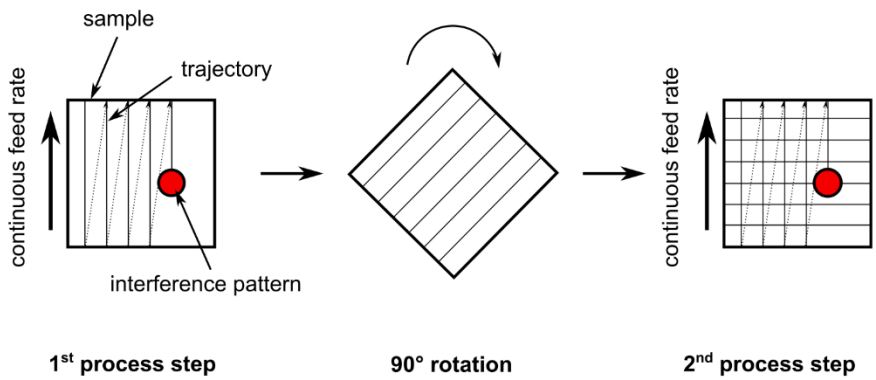

Fig. 3: Process strategy for DLIP treatment. To reach a 2D-structure with 1D-line interference pattern 2 steps were performed. After structuring in one direction, the sample was rotated by 90° to structure the sample perpendicular to the first step.

2.3. Material

Mirror-polished 316L stainless steel samples were used for all DLIP experiments. Their chemical composition is given in Table *1*. The experiments were performed by treating the entire sample surface with a size of 50x50mm^2. Control samples had the same material and size and an untreated surface with a roughness of 0.37µm.

Table 1: Chemical composition of 316L (stainless steel) in %

C	Mn	Si	Cr	Ni	Mo	P	S	Ni	Fe
0.03	2	0.75	16 – 18	10 – 14	2 – 3	0.045	0.03	0.1	Bal.

2.4. Topography analysis

The topography of the DLIP-treated surfaces was magnified with a JEOL JSM-6490LV scanning electron microscope (SEM) to determine the size, geometry and homogeneity of the structure.

2.5. Bacterial retention

For bacterial retention quantification, three identical treated samples and three untreated control samples were compared. Each structure type was quantified with the two bacteria types, E. coli and S. aureus. The examination was performed according to the ISO standards for the measurement of antibacterial performance [25,26] and is described in detail in [8]. To ensure that the bacterial cells were free from environmental stresses and in an appropriate growth stage, the preparation of the bacterial solutions with E. coli (ATCC 8739) and S. aureus (ATCC 6538P) was undertaken in conformance with ISO 27447. After diluting the stock to 1/500, the cell density results to 2.6x10^7 cfu/ml for E.coli and 8.2x10^6 cfu/ml for S.

aureus. Laser-treated and control surfaces were cleaned with acetone (15 minutes), sterilized with pure ethanol (10 minutes) and dried in air for 10 minutes in a UV hood. After the contact of the surfaces with the bacterial cells at 24°C for two two hours, excess liquid was eliminated from the samples by holding the samples in a vertical position for two minutes. Swabs were then taken in both orthogonal directions along each surface and incubated prior to quantification of the number of colony-forming units per swab by means of a colony counter.

3. Results

3.1. Topography analysis

Fig. 4 shows the resulting topographies in two different magnifications from the SEM, 5000x and 20000x, respectively. The upper topographies ((a) and (b)) result from the p-polarization setting on the optical setup, as represented in Fig. 1. The topographies below from the s-polarization setting. Despite the identical intensity distribution, the topographies have a clear difference, depending on the polarization. This effect is due to the formation of Laser Induced Periodic Surface Structures (LIPSS), which occur parallel to the polarization. With p-polarization, the LIPSS occur parallel to the interference lines and appear to have a minor effect on the topography that leads to the expected ablation of grooves in vertical and horizontal direction after the two process steps, as described in section 2.2. This topography resembles a grid with sunken grid bars, which are referred to as cones in the following. However, with s-polarization, the LIPSS occur perpendicular to the interference lines and gain influence on the topography. This fact causes the topography to resemble a grid with raised grid bars. This effect was investigated by [19] for structures with a period range of 1.4 – 6.3 µm. This topography is referred to as holes in the following. Nevertheless, both topographies have a period of about 850 nm, consistent with the theoretical period from eq. (2).

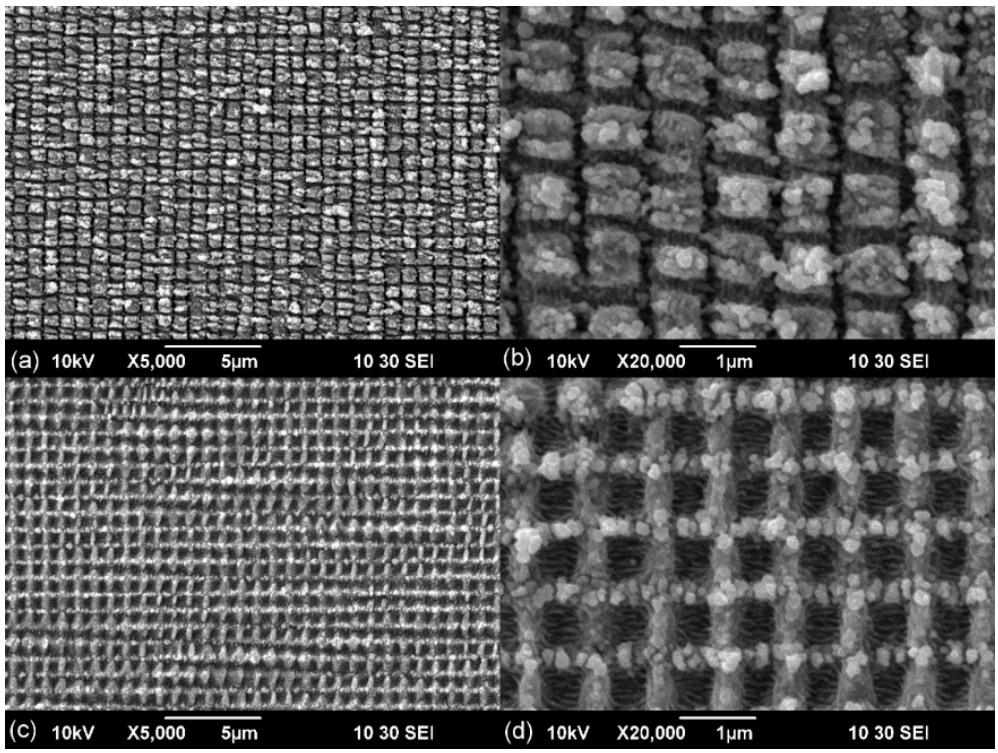

Fig. 4: Raster electron microscope (REM) images of the resulting topographies after DLIP laser-treatment. The upper images show the structure after treatment with p-polarization setting, referred to as cones in the text. The images below shows the structure after s-polarization treatment, referred to as holes in the text. Two different magnifications of 5000x and 20000x are pictured on the left and right hand side, respectively. Both topographies result after the 2 step processing strategy, described in section 2.2.

3.2. Bacterial retention

Fig. *5* represents the residual bacteria count after two hours exposure of the cone and hole topography to the bacterial solutions. The values are normalized against the bacteria count of untreated control samples with an areal surface roughness of 0.37 µm. The values show a significant reduction of the bacteria retention. A reduction of 99.8% and 99.4% for E. coli on cones and holes, respectively, was measured. In the case of S. aureus the reduction was 70.6% and 79.1% on cones and holes, respectively.

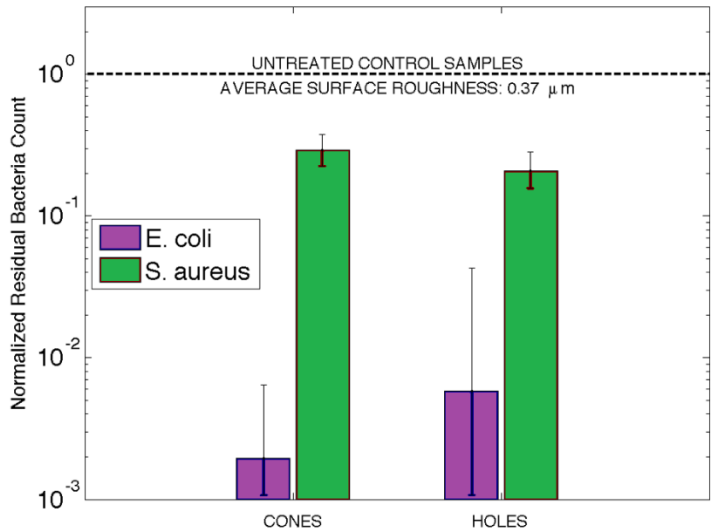

Fig. 5: Residual Bacteria Count, normalized to untreated surfaces. The diagram shows the measured reduction of bacterial retention. A reduction of 99.8% and 99.4% for E. coli on cones and holes, respectively, could be measured. In the case of S. aureus the reduction was 70.6% and 79.1% on cones and holes, respectively.

4. Conclusion

This work shows that the Direct Laser Interference Patterning with two interfering beams is a suitable method to produce antibacterial surfaces on stainless steel. Despite the linear dependence of the period of the produced structures on the laser wavelength, sub-micrometer period of about 850 nm could be realized with a wavelength of 1030 nm. This was possible with an incidence angle of 37° to the surface normal. To avoid melting effects, an ultrafast laser with a pulse duration of 8 ps was employed. The polarization dependent influence of Laser Induced Periodic Surface Structures was employed to generate two different topographies. This was realized with a p-polarization and s-polarization setting. Due to the period of the LIPSS, which is close to the laser wavelength, cones and holes structure occurred at p- and s-polarization, respectively, despite the identical interference pattern. Both topographies were examined for their antibacterial behavior in the case of E. coli and S. aureus. Three surfaces with a size of 50x50mm^2 each were structured for this purpose. The examination was carried out in accordance with the ISO standards for the measurement of antibacterial performance. Compared to untreated control surfaces a reduction of 99.8% for E. Coli and 79.1% for S. aureus could be measured. Due to the high power capability of the optical setup, higher structuring rates can be achieved in the future.

Acknowledgements

This project has received funding from the European Union's Horizon 2020 Research and Innovation Programme under Grant Agreement No. 687613 (www.tresclean.eu). The authors would like to thank Alessandra Carletti (Artest – Laboratori e Servizi – S.p.A.) for her assistance in developing and performing the bacterial adhesion tests.

References

[1] Srey S, Jahid IK, Ha S-D. Biofilm formation in food industries: A food safety concern. Food Control 2013;31:572-85.

[2] Isaacs MA, Durndell LJ, Hilton AC, Olivi L, Parlett CMA, Wilson K, et al. Tunable Ag@SiO2 core-shell nanocomposites for broad spectrum antibacterial applications. RSC Advances 2017;7:23342-7.

[3] Meireles A, Borges A, Giaouris E, Simões M. The current knowledge on the application of anti-biofilm enzymes in the food industry. Food Research International 2016:86:140-6.

[4] Linklater DP, Juodkazis S, Ivanova EP. Nanofabrication of mechano-bactericidal surfaces. Nanoscale 2017;9:16564-85.

[5] Epperlein N, Menzel F, Schwibbert K, Koter R, Bonse J, Sameith J, et al. Influence of femtosecond laser produced nanostructures on biofilm growth on steel. Applied Surface Science 2017;418B:420-4.

[6] Fadeeva E, Truong VK, Stiesch M, Chichkov BN, Crawford RJ, Wang J et al. Bacterial retention on superhydrophobic titanium surfaces fabricated by femtosecond laser ablation. Langmuir 2011;27:3012-9.

[7] Rajab FH, Liauw CM, Benson PS, Li L, Whitehead KA. Picosecond laser treatment production of hierarchical structured stainless steel to reduce bacterial fouling. Food and Bioproducts Processing 2018;109:29-40.

[8] Lutey AHA, Gemini L, Romoli L, Lazzini G, Fuso F, Faucon M, et al. Towards laser-textured antibacterial surfaces. Scientific Reports 2018;8:10112.

[9] Kietzig A-M, Hatzikiriakos SG, Englezos P. Patterned superhydrophobic metallic surfaces. Langmuir 2009;25:4821-7.

[10] Bonse J, Höhm S, Kirner SV, Rosenfeld A, Krüger J. Laser-induced periodic surface structures – a scientific evergreen. IEEE Journal of Selected Topics in Quantum Electronics 2017;23:9000615.

[11] Gemini L, Faucon M, Romoli L, Kling R. High throughput laser texturing of super-hydrophobic surfaces on steel. Proc. SPIE 2017:10092.

[12] Gnilitskyi I, Derrien TJ-Y, Levy Y, Bulgakova NM, Mocek T, Orazi L. High-speed manufacturing of highly regular femtosecond laser-induced periodic surface structures: Physical origin of regularity. Scientific Reports 2017;7:8485.

[13] Tsibidis GD, Fotakis C, Stratakis E. From ripples to spikes: A hydrodynamical mechanism to interpret femtosecond laser-induced self-assembled structures. Physical Review B 2015;92:041405(R).

[14] Daniel C, Mücklich F, Liu Z. Periodical micro-nano-structuring of metallic surfaces by interfering laser beams. Applied Surface Science 2003;208-209:317-21.

[15] Tan B, Sivakumar NR, Venkatakrishnan K. Direct grating writing using femtosecond laser interference fringes formed at the focal point. J. Opt. A: Pure Appl. Opt. 2005;7:169-74.

[16] Lasagni AF, Roch R, Langheinrich D, Bieda M, Wetzig A. Large area direct fabrication of periodic arrays using interference patterning. Physics Procedia 2011;12:214-20.

[17] Huang J, Beckemper S, Gillner A, Wang K. Tunable surface texturing by polarization-controlled three-beam interference. J. Micromech. Microeng. 2010;20:95004.

[18] Alfredo I. Aguilar-Morales, Sabri Alamri, Andrés Fabián Lasagni. Micro-fabrication of high aspect ratio periodic structures on stainless steel by picosecond direct laser interference patterning. Journal of Materials Processing Tech. 252 (2018) 313-321

[19] Sabri Alamri, Fotis Fraggelakis, Tim Kunze, Benjamin Krupop, Girolamo Mincuzzi, Rainer Kling and Andrés Fabián Lasagni. On the Interplay of DLIP and LIPSS Upon Ultra-Short Laser Pulse Irradiation. Materials 2019, 12, 1018

[20] Negel P, Loescher A, Voss A, Bauer D, Sutter, Killi A, et al. Ultrafast thin-disk multipass laser amplifier delivering 1.4 kW (4.7 mJ, 1030 nm) average power converted to 820 W at 515 nm and 234 W at 343 nm. Optics Express 2015;23:21064-77

[21] Nubbemeyer T, Kaumanns M, Ueffing M, Gorjan M, Alismail A, Fattahi H, et al. 1 kW, 200 mJ picosecond thin-disk laser system. Opt. Lett. 2017;42:1381-4.

[22] Graf T. High-productivity materials processing with ultrafast lasers. Journées nationales des procédés Laser pour l'industrie; 2017 Sep 14; Strasbourg, France

[23] Peter A, Onuseit V, Freitag C, Faas S, Graf T. Flexible, compact and picosecond laser capable four-beam interference setup. Laser in Manufacturing; 2017 June 26-29; Munich, Germany

[24] Helbig R, Günther D, Friedrichs J, Rößler F, Lasagni A, Werner C. The impact of structure dimensions on initial bacterial adhesion. Biomaterials Science 2016;4:1074-8.

[25] ISO 22196 Measurement of antibacterial activity on plastics and other non-porous surfaces. International Organization for Standardization; 2011.

[26] ISO 27447 Fine ceramics (advanced ceramics, advanced technical ceramics) – Test method for antibacterial activity of semi-conducting photocatalytic materials. International Organization for Standardization; 2009.